Deep–Sea Research I 205 (2024) 104236

Contents lists available at ScienceDirect

Deep-Sea Research Part I

journal homepage: www.elsevier.com/locate/dsri

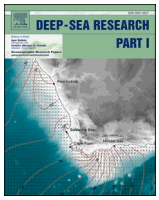

Inferring benthic megafaunal sediment reworking activity in relation to bottom water oxygen in Barkley Canyon, NE Pacific from video and acoustic imaging analysis

Alessia C. Ciraolo [a,*], Paul V.R. Snelgrove [a,b], Douglas Schillinger [c], Fabio C. De Leo [d,e]

[a] Department of Ocean Sciences, Memorial University of Newfoundland, 0 Marine Lab Road, St. John's, NL, A1C 5S7, Canada
[b] Department of Biology, Memorial University of Newfoundland, 232 Elizabeth Ave, St. John's, NL, A1B 3X9, Canada
[c] Bedford Institute of Oceanography, Fisheries and Oceans Canada, Dartmouth, NS, Canada
[d] Ocean Networks Canada, University of Victoria, 100-2474 Arbutus Road, Victoria, BC, V8N 1V8, Canada
[e] Department of Biology, University of Victoria, PO Box 3080, Victoria, BC, V8W 2Y2, Canada

A B S T R A C T

Sediment reworking activity influences benthic functioning expressed as nutrient fluxes and carbon cycling. Multiple studies have addressed sediment reworking based on observations from individual instrument types (e.g., video camera, side-scan sonar, multibeam), but none have considered reworking based on two or more complementary instruments. We therefore analyzed deep-sea megafaunal and reworked sediment traces by combining and comparing observations from non-invasive instruments, an underwater video camera and a rotary sonar, as part of the node of Ocean Networks Canada's NEPTUNE cabled observatory, located at 396 m depth in Barkley Canyon Upper Slope, NE Pacific Ocean. Specifically, we examined sediment traces and benthic megafaunal communities during two different sampling periods (May and September 2013) and at two different spatial scales of analysis. The camera images (~0.5 m^2) documented significantly lower megafaunal density during the period of reduced oxygen concentrations (May). Although we did not observe significant differences in sediment trace diversity and density between the two study periods, we were interested in how the relief traces generated by unidentified gastropods (likely the family Solariellidae) influenced sediment mixing. Relief traces showed higher density in low oxygen (May, 1.87 count m^{-2}) than in high oxygen (September, 1.17 count m^{-2}) conditions. Sonar images (~1268 m^2), which lacked sufficient resolution to allow identification of benthic organisms, documented distributions of biological pits (regions of low backscatter), a significantly greater proportion of bioturbated seafloor area, and increased in pit size with increased oxygen levels. Pits dominated sonar images at this location and persisted through the two study periods. Most sonar field of view subsections showed a significant increase in circularity of pit shapes, likely explained by increased reworked sediment with increasing oxygen concentration. We conclude that, except for relief burrows, higher reworked sediment area coincided with the highest oxygen concentration, which aligns with previously established reduced metabolic activity by benthos adapted to oxygen minimum zones. Furthermore, we emphasize the complementarity of the two imaging techniques (video and sonar) in understanding deep-sea benthic ecosystem dynamics, as well as the importance of considering multiple spatial scales when investigating proxies of bioturbation activity.

1. Introduction

The cost and logistical challenges of deep-sea research (Smith et al., 2022) have motivated researchers to develop novel tools to enable remote and *in-situ* time-series data collection. In recent decades, cabled ocean observatories have offered a greater array of tools to study short and long-term Earth-ocean processes (e.g., Vardaro et al., 2013; De Leo et al., 2018; Aguzzi et al., 2019; Aguzzi et al., 2020; Lopez-Vazquez et al., 2020). For example, Canada's VENUS (Victoria Experimental Network Under the Sea) and NEPTUNE (North-East Pacific Undersea Networked Experiments) observatories, collectively known as Ocean Networks Canada (which also includes observatories in the Arctic and Atlantic Oceans), have collected data remotely from the coast to the deep-sea of the Northeast Pacific Ocean for over a decade (Barnes et al., 2007). These observatories link numerous and diverse sets of sensors through cables, connectors, and instrument platforms (Barnes et al., 2007).

Previous studies on spatial heterogeneity of deep-sea biodiversity, nutrient cycling, and the roles of phytodetritus, scavengers, and carcass falls have utilized remotely operated vehicles (e.g., Campanyà - Llovet et al., 2017; Miatta and Snelgrove, 2021), benthic landers (e.g., Witte et al., 2003; Sweetman and Witte, 2008) and cabled observatories (Thomsen et al., 2017; De Leo et al., 2018). Of these tools, cabled observatories offer the best opportunity for continuous time series and even real-time observation of processes such as bioturbation – the mixing of sediment particles by biological activity (Kristensen et al.,

* Corresponding author.
E-mail address: acciraolo@mun.ca (A.C. Ciraolo).

https://doi.org/10.1016/j.dsr.2024.104236
Received 27 July 2023; Received in revised form 8 December 2023; Accepted 10 January 2024
Available online 11 January 2024

2012) – that leads to biogenic transport of pore water and changes in physical and chemical properties of sediment (Shull, 2009). Bioturbation, directly and indirectly, affects nutrient fluxes, oxygen penetration depth, dispersion of contaminants, and particularly the process of organic matter mineralization near the sediment-water interface (Kristensen, 2000; Furukawa et al., 2001).

Low oxygen concentration in bottom-water (defining hypoxia as $0 < O_2 < 1.4$ ml l^{-1}, Ekau et al., 2010) also influences bioturbation and the consequences of bioturbation, often by decreasing megafaunal or macrofaunal biodiversity (e.g., Smith et al., 2000; Levin, 2003; Belley et al., 2010) and changing bioturbator behavior and activity (Sturdivant et al., 2012; Riedel et., 2014). However, a lack of opportunities for repeat observations limits our knowledge of oxygen concentration effects on bioturbation along continental margins (Robert and Juniper, 2012). Along with water depleted of O_2, grain size distributions, and sediment permeability to fluid flow influence sediment mixing (reviewed by Shum and Sundby, 1996; Huettel and Webster, 2001), which add to the complexity of understanding benthic ecosystem functions (Snelgrove et al., 2014) such as biogeochemical cycling processes.

Bioturbation often leaves a variety of types of visible traces on the seafloor known as "*lebensspuren*", a German term for life traces (Mauviel and Sibuet, 1985; Bell et al., 2013). Some of these traces, which include "pits" and "mounds", refer to seabed formations that originate from biological activity. Macrofauna form pits to avoid predators, capture prey (Auster et al., 1995), or through feeding activities of deposit feeders (Nowell et al., 1984). Mounds refer to sediment defecated by macrofauna back to the surface, which can coil into characteristic fecal mounds (Kukert and Smith, 1992). Traces are also classified according to their morphology in surface-traces and relief-traces (Mauviel and Sibuet, 1985). Surface traces refer to features created by mixing sediment in the upper few millimeters or centimeters of the sediment, in contrast to relief traces created by animals mixing deeper sediment layers and bio-irrigating (Belley et al., 2010). Changes in size and shape of pits, a type of large-scale of relief traces, can indicate enhanced sediment reworking or hydrodynamic activities (Hay and Wilson, 1994; DuVal et al., 2021). Changes in pit morphology may occur in environments with moderate currents and pit aspect ratios (depth/diameter) between 0.5 and 2 because particle fluxes and particle residence time increase (Yager et al., 1993). Consequently, the increased particle flux and vortex at pit walls can increase bio-irrigation, elevating labile organic matter content in the pit and attracting more organisms, further increasing sediment mixing. Given the appropriate geometry, a single beam rotary sonar is well suited to detect relief traces of scales on the order of the radial range bin size, and the range-dependent arc traced by each mechanical step (Jones and Traykovski, 2018). Single beam sonars represent pits via the acoustic shadow cast by the leading edge of the pit. The length of the shadow relates to the pit depth and its aspect ratio. In saome cases, the far edge of the pit may return elevated signal intensity depending on geometry.

Past studies assessed bioturbation in different ways, based on habitat characteristics and organisms present, and considered the time scales of mixing. For example, researchers have used invasive techniques for direct collection of sediment and bioturbation features and structures. Those methods include castings (Cadée, 1976; Seike et al., 2012), entrapment (Rhoads, 1963; Maire et al., 2008), and levelling (Cadée, 1976; Maire et al., 2008; Seike et al., 2012). The quantification of either natural (e.g., radionuclides) or added (e.g., luminophores) (Wheatcroft, 1991; Maire et al., 2008) tracers offers another mechanism to assess the vertical movement of particles within sediments. Surface image analysis, a non-destructive approach, offers an alternative method to assessing short-term temporal changes in sediment reworking. For example, Robert and Juniper (2012) used a real-time camera to monitor bioturbation by flatfish, echinoderms, and gastropods, and to estimate the time required for organisms to turn over surface sediments. Belley et al. (2010) used video imagery to quantify bioturbation in the Gulf of Lawrence by quantifying surface relief of traces left by biological activity on the sediment surface. Solan and Kennedy (2002) and Solan et al. (2004) used a sediment-profile image camera (SPI) to provide in-situ, undisturbed cross-sectional images of the benthos (Rhoads and Cande, 1971), and to quantify numbers of biogenic structures (tubes, burrows, oxic voids, feeding pits), numbers of epi- and infauna, and maximal depths of oxic voids within the sediment column (Lamarque et al., 2021). Coupling this technique with others, such as luminophores addition or the use of a flexible software such as AVIExplore for automated video analysis (Romero-Ramirez et al., 2016), enables visual identification of species and provides quantifiable information on infaunal activity.

Other than as a tool to quantify megafaunal composition over large spatial scales, relatively few studies have used non-destructive sonar imaging to quantify bioturbation activity (Robert and Juniper, 2012). Sonar images, in tandem with continuous video, have been used to study trawling impacts on the seabed (De Leo et al., 2017), to analyze pit formation in relation to seafloor roughness (DuVal et al., 2021), and to study nearshore bedform development following a storm and in response to changes in wave direction (Hay and Wilson, 1994; Maier and Hay, 2009).

Given the limited studies that compared video and sonar images to evaluate deep-sea reworked sediment and traces as proxies of bioturbation activity, assessing the advantages, limitations, and complementarity of video and sonar images can potentially enhance the toolbox available for bioturbation studies. Therefore, our study aimed to combine and compare the two methodologies. Such non-destructive techniques augment the potential for long-term sustained observation aligned with monitoring of ecosystem biodiversity and function. Moreover, we also assessed reworked sediment traces and pit formation over small spatial scales (cm to 20s of m) in response to periods of contrasting bottom-water oxygen concentration levels on the upper continental slope. Specifically, using video images, we examine density and diversity of benthic megafauna, sediment traces, and total bioturbated area over time. In parallel, we assessed bioturbated seafloor based on sonar images by examining the number of pits and the total area covered by pits during different times of the year. Finally, because we hypothesized that changes in pit features may result from biological or hydrodynamic factors in concert, our study also addresses changes in pit features, specifically in terms of circularity and diameter.

2. Materials and methods

Barkley Canyon, a continental slope feature located 100 km off the coast of Vancouver Island, has a backbone fiber optic cable - part of the Ocean Networks Canada (ONC) cabled observatory (Barnes et al., 2007) - that sends real-time data to a shore station in Port Alberni, British Columbia, and onward to the University of Victoria (Fig. 1 A). At the Barkley Canyon Upper Slope (BCUS) sampling site, an instrument platform (IP) deployed at 396 m depth has been connected to the observatory network since May 2009 (Fig. 1 B).

We measured bottom-water column characteristics and *in-situ* oxygen concentrations using a Conductivity-Temperature-Depth (CTD) profiler (Sea-Bird SeaCAT SBE16plus V2 7029) and a dissolved oxygen sensor (Sea-Bird SBE 63 Dissolved Oxygen Sensor 630110), respectively, both ~1.5 m high above the bottom (HAB) (see Fig. 2; Supplementary Table 1). These data were collected at a rate of 1 measurement/minute.

In 2012–2013 the platform at Barkley Canyon Upper Slope was equipped with two upward-looking Acoustic Doppler Current Profilers, one 300 kHz unit, and one 2 MHz Aquadopp profiler equipped with a right-angle head. The 2 MHz system was mounted on a flat, low profile secondary platform, in contrast to the 300 kHz unit mounted on the main platform approximately 2 m above the sea floor. An ROV deployed this secondary platform near (<5 m) the main lander. The low-profile platform and right-angle head configuration of the profiler enabled near-bottom measurements from 10 cm height above the seabed to 150 cm HAB. We present data from the 2 MHz unit to investigate sediment

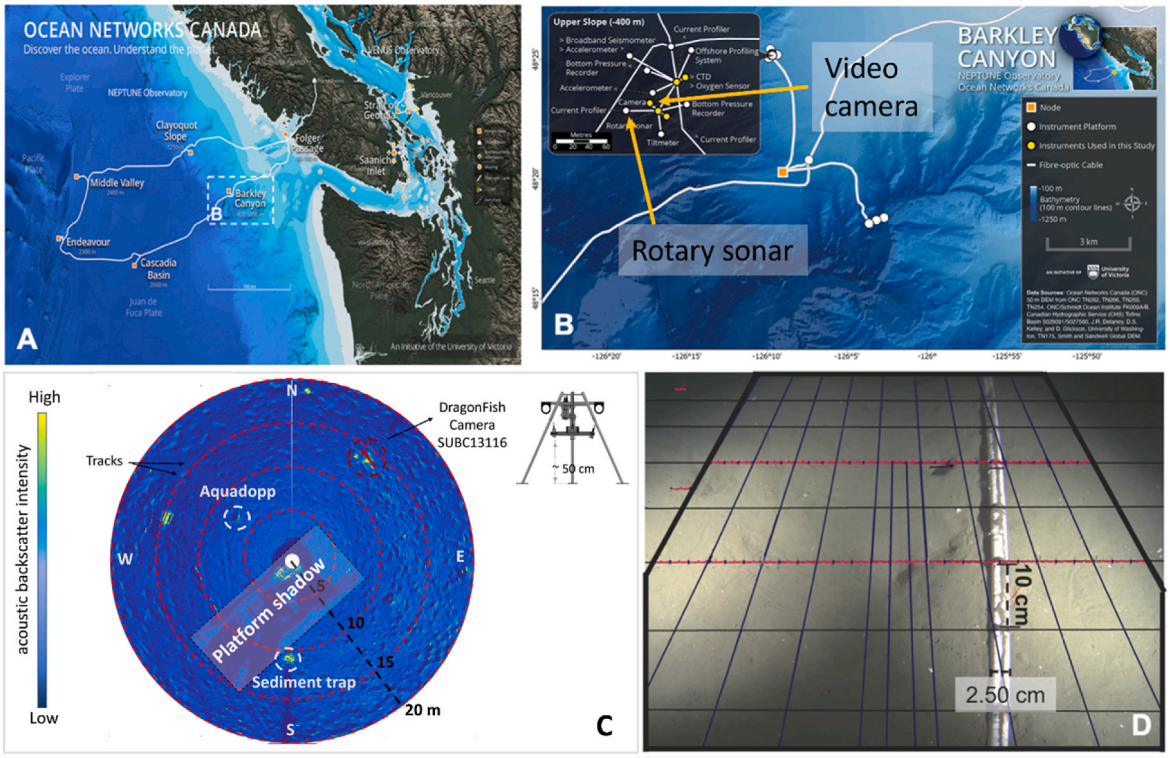

Fig. 1. A) Ocean Networks Canada cabled observatory off Vancouver Island, NE Pacific; B) Barkley Canyon Upper Slope location highlighting the positioning of all instruments used in the study; C) Example of the Kongsberg Mesotech Rotary Sonar (Table 1) 360° sweep image covering a 20-m radius field of view (FOV), indicating the relative positions of the video camera (placed approximately 10 m away from the main instrument platform using a Remotely Operated Vehicle (ROV)), and labelling prominent high acoustic backscatter targets and associated shadow zones such as the Aquadopp, sediment trap, and instrument platform in the center of the image (the image is oriented with respect to true north); D) SubC Dragonfish SUBC13116 video camera (mounted on a galvanized steel tripod) field of view with overlaid perspective grid for scaling, created using the program GIMP (GIMP Development The GIMP Development Team, 2019), and using geometry based on the height of the lens above the seafloor (45 cm), the lens' aperture angles, a = 34.5 (vertical) and b = 53.3 (horizontal), as described in Command et al. (2023), and a 1-m long white PVC pipe marked at 10-cm intervals placed on the seafloor perpendicular to the long axis of the imaging platform, with one end directly below the camera on the seafloor (Nadir point).

resuspension and mobilization. The 2 MHz Aquadopp sampled at 10 s intervals, and we present data averaged over 15-min periods. In order to evaluate near-bottom flow, but away from any flow disturbance caused by the instrument platform, we selected data from the 10th bin (21 cm HAB) for the directional histogram shown in Supplementary Fig. 1.

We summarize the two methodological approaches, highlighting which scales and factors we analyzed to address our main questions from video and sonar images, respectively (Table 2); the sub-sections below provide more details.

2.1. Reworked sediment characterization using an underwater video camera

2.1.1. Benthic community and sediment traces

We followed Belley et al. (2010) in determining the number of images to analyze in our study. Specifically, by plotting species-trace accumulation curves and calculating the mean and variance of the accumulated species and traces, they concluded that analysis of 15 images sub-sampled randomly from 157 would be sufficient to evaluate species and trace distributions without significantly affecting their conclusions. Accordingly, we analyzed 14 of 168 images per month.

Within the video frames, we identified and enumerated benthic megafaunal organisms to the lowest feasible taxonomic level. We calculated alpha biodiversity and densities (by dividing abundance by the surface area of the analyzed field of view (~0.5 m^2)). Consequently, we did not count any fauna outside the ~0.5 m^2. We calculated reworked sediment by measuring the sizes of benthic organisms and traces using a perspective grid. We separated traces into surface and relief categories, which we then separated into sub-groups (Jones et al., 2007; Belley et al., 2010). The surface traces included organisms, organism imprints, ploughs, trails, and depressions, whereas the relief traces included small burrows (0.5–1 cm), medium burrows (1–5 cm), and large burrows (>5 cm) (Belley et al., 2010). We specifically measured surface, relief, and total trace (surface + relief traces) density and diversity. For each trace category, we measured density as the number of traces divided by the surface area of the analyzed field of view, and calculated trace diversity components.

2.1.2. Estimating total reworked sediment area

We measured the bioturbated area as the total area covered by both surface and relief traces. To obtain an estimate of the total area of burrow openings, we averaged the area covered by small and medium burrows for each period. To calculate the area covered by small burrows for periods with contrasting oxygen concentrations, we multiplied the average small burrow area by the number of small burrows. We determined the area of small or medium burrow openings by approximating the opening as a circle ($A = \pi r^2$). We included the area of seafloor occupied by benthic macrofauna, trails, and ploughs in the area covered by surface traces because organisms were presumably forming traces at the time the image was taken.

In "Video editor", we measured the time that small and medium burrows persisted by creating time-lapse videos from screenshots taken from every subsample video image collected daily.

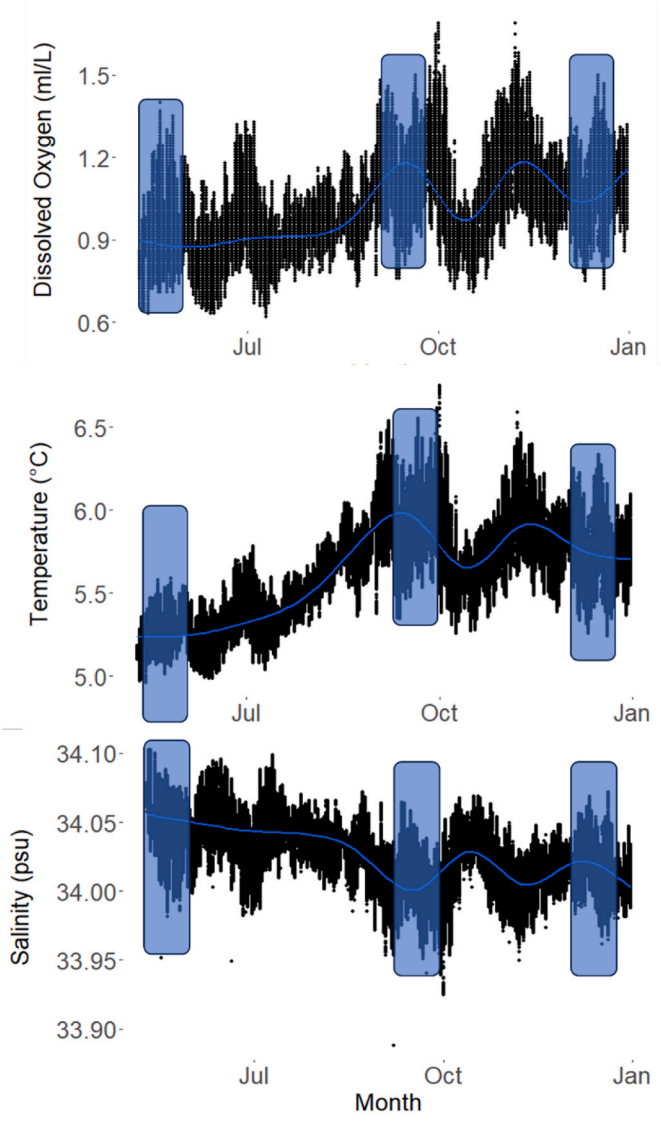

Fig. 2. Oxygen concentration, temperature, and salinity data from May to December 2013. Blue squares indicate the time windows analyzed for this study. Data from January to May 9th were not available. The blue line connects average daily values of oxygen, temperature, and salinity, respectively, which we used to establish the minimum and maximum O_2 peaks of the year.

Table 1
Characteristics of the sonar head.

Sonar characteristics	
Rotary step size	0.225°
Beam width	0.9°
Range resolution[a]	1.95 cm
Frequency	675 KHz

[a] The resolution of a sonar image limits the size of the smallest detectable object. Therefore, the coarser the resolution (e.g. > 1 cm), the harder it is to detect small objects (Hay and Wilson, 1994).

2.2. Reworked sediment characterization using rotary sonar

We analyzed pits from their shadows, represented visually by black spots in the sonar images. The shadows, or balck spots, represent lower acoustic backscatter intensity.

Table 2
Spatial scale, technical, biological, and sedimentary variables analyzed through video and sonar images. "N.A." indicates a specific variable not analyzed from the specific instrument. *BWO_2* refers to bottom water oxygen concentration.

	Video Images	Sonar Images
Spatial scale	~0.5 m^2	~1268 m^2
Type of instrument	Color high-definition fixed camera	Rotary Sonar
Analyzed period	May 18–31 and September 20 - October 5, 2013	May 20–30, September 20 30, and December[a] 20–31, 2013
BWO_2 concentration	May 0.8 ml l^{-1} ± 0.12 (SD), September 1.3 ml l^{-1} ± 0.18 (SD) (Fig. 2)	May 0.8 ml l^{-1} ± 0.12 (SD), September 1.3 ml l^{-1} ± 0.18 (SD), December (1.09 ml l-1 ± 0.11 (SD)). (Fig. 2)
Video recordings stored	Ocean Networks Canada's Oceans 3.0 data archiving system. (https://data.oceannetworks.ca/DataSearch)	Ocean Networks Canada (https://data.oceannetworks.ca/DataSearch)
Video and sonar duration	5 min recorded every 2 h per d^{-1}	Collected 5 sonar sweeps h^{-1}. One sweep takes approximately 4 min
Video and sonar processing		
Analyzed videos	1 video choose randomly per day to avoid pseudo-replication (Belley and Snelgrove, 2017), and to avoid the period when the light was off. 14 videos in total per sampling period	1 composite sonar image per day presented as an average of the sweeps that sonar collected every 4 min 10 images in total per sampling period
Analyzed video sequences	1 min (from ~2 min 30s to ~3 min 30s) out of every 5 min of each video (Chauvet et al., 2018)	NA
Biological variable	Megafaunal diversity and density	N.A.
Sedimentary variable	*"Lebensspuren"* or bioturbation traces (superficial and relief)	Pits
Sedimentary variable	Traces diversity and abundance Averaged reworked sediment area (from sediment traces) N.A.	Number, circularity, and diameter of pits Averaged reworked sediment area (from pits) Platform traces refilling as indices of either hydrodynamic or biological or both activities

[a] We included data from December because pit shapes change little over time, and December data strengthened this comparison.

2.2.1. Counting of pits

To count the number of pits, we analyzed daily averaged sonar images collected from May 20–30, and September 20–30, 2013, using Image J software 1.8.0 (freely available, https://imagej.nih.gov/ij, Rasband, 1997), eliminating the shadow from the frame supports, the sediment trap, and the camera frame (which appears in the same location in each image as yellow spots, indicating high backscatter returns from the instrument itself). We also eliminated the acoustic shadow "behind" the instruments. We completed the following steps to enumerate the pits (Fig. 3): (1) image 'binarization', from color to grayscale (8-bit transform); (2) 'thresholding', generating a binary image from bi-chromatic grayscale image; (3) elimination of extra shadows such as the platform and sediment trap shadows; (4) analyze and count visual features selecting feature size (shadow zones) between 0.2 and infinity in m^2, without fitting any specific feature shape. The threshold and size limit steps were imposed to restrict the impact of noise (Fig. 3 C), acknowledging that this filtering may exclude some pits, while not eliminating all noise.

2.2.2. Estimating total bioturbated area

We calculated the reworked sediment area as the average area of pits

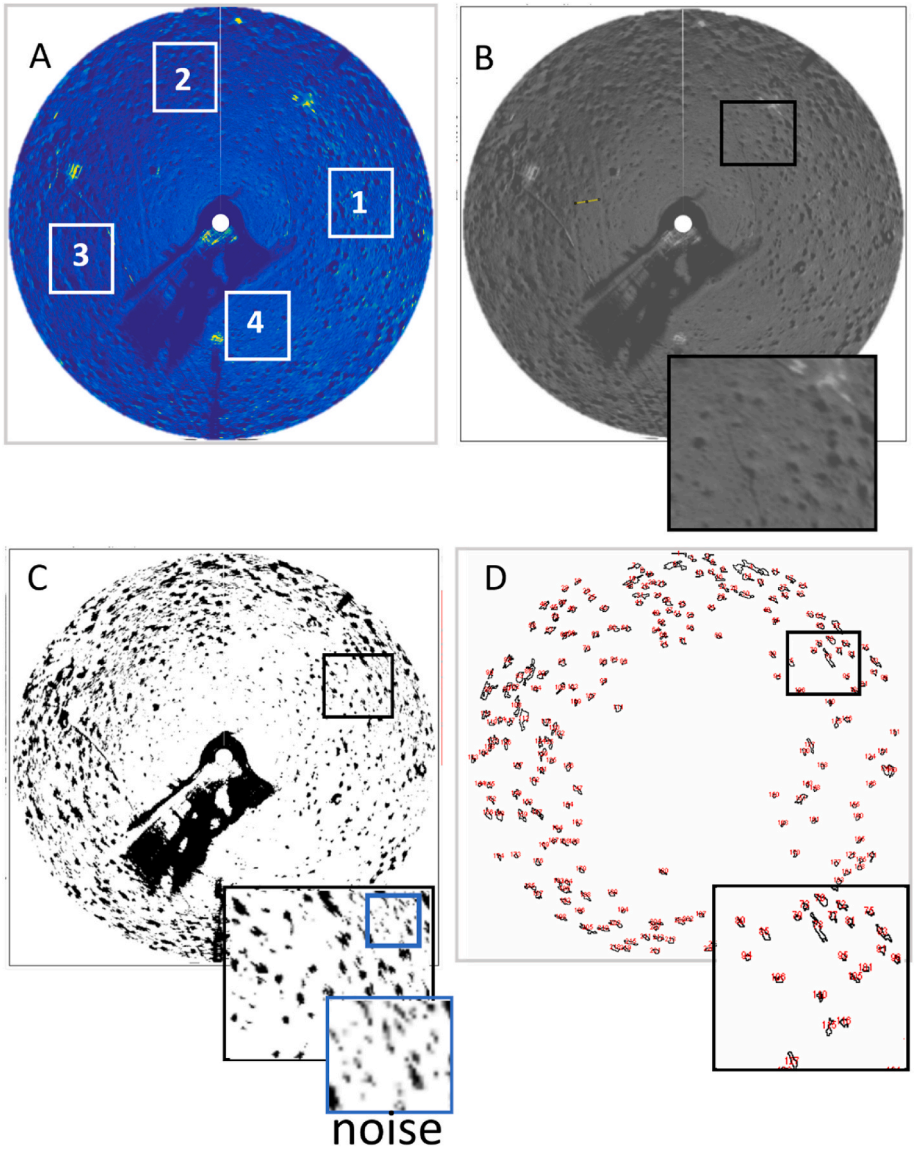

Fig. 3. Summary of steps performed by the automated image analysis protocol: A) Original image. The four white boxes indicate the four sub-sections used to evaluate pit features; B) 8-bit grayscale image; yellow line refers to distance (3 m) between seafloor marks; C) Thresholding – zoomed-in blue box exemplifies area impacted by "noise" (particles <0.2 at a set scale of 1 m^2); D) Count features based on chosen size and shape. Black boxes indicate a zoomed-in sub-section area.

measured by ImageJ using the algorithm described in 2.2.1 (Fig. 3). For comparison to ambient sediment reworking, we calculated estimates of infilling of two parallel tracks (Section 2.3). Ambient refers to the combination of physical processes driven by ocean currents and small-scale biological processes not resolvable at the resolution of the sonar (ie not pits). These tracks were visible on the left side of each sonar image for both bottom-water oxygen concentration scenarios. This interpretation is consistent with a fishing trawl 'hit' event that took place in February of 2011. Based on archived rotary sonar images, these seafloor track marks only appeared after May 2011 (F. De Leo, pers. obs.). Thus, the long-term persistence and changes in the backscatter strength signals of these tracks provide an indicator of how the combined effects of bottom current hydrodynamics and bioturbation can mobilize sediments and refill irregular seafloor depression areas.

2.2.3. *Measuring pit shape*

To analyze the shape of the pits we focused on the circularity and diameter descriptors provided by ImageJ. Here, circularity refers to 4π*area/perimeter^2. A value of 1.0 indicates a perfect circle and a value approaching 0.0 indicates an increasingly elongated shape, noting that circularity values may be invalid for very small objects. Diameter refers to the longest distance between any two points along the selection boundary.

We looked at the bioturbation feature size descriptors over the 20-m radius sonar FOV images and in four selected subsections (Fig. 3 A) and compared the May, September, and December 10-d sampling periods. We selected the sonar image FOV subsections to identify whether bioturbation feature sizes changed uniformly across the entire area of the seafloor imaged by the sonar. These selected subsections were deliberately set to avoid inclusion of instrument platforms, instrument shadows, or sediment disturbances caused by platform tracks, thus avoiding underestimation of reworked sediment area measurements. For the four subsections, we set the threshold as described above (Fig. 3), and set the circularity range from 0.0 to 1 for subsections 1 and 4, and from 0.2 to 1 for subsections 2 and 3. The latter two showed different mean elevated backscatter (noise).

2.3. *Estimating seafloor marks residence time*

The two long and linear seafloor scar marks (i.e. tracks) described

above provided a proxy for both the persistence and transformation of bioturbation marks caused by benthic megafauna. The scars were clearly visible in the west sector of all analyzed rotary sonar images. In this specific case, we used the platform tracks as indicators of sediment refilling rates of megafaunal pits, which were challenging to detect through the sonar images that could not provide measures of bedform height/depth individually. In addition, deeper tracks accumulate more sediment along the track edge, narrowing the track width. The opposite effect occurs when sediment refills the platform track. Accordingly, we measured the width of each track by initially choosing six points at random along the track in the first images of May, subsequently reducing sampling to three points by the last images of December (Supplementary Fig. 2) because the visual distinctiveness of the points decreased over time. We selected points equidistant from one another (Supplementary Fig. 2).

2.4. Statistical analysis

2.4.1. Video data analysis

We calculated density for benthic megafaunal communities and univariate indices including Shannon - Wiener diversity index (H′), Simpson's index, Pielou's evenness index (J′), and species richness (S) based on non-transformed megafaunal densities for both bottom-water oxygen concentration scenarios, as well as sediment trace density (%), and diversity.

We used a stepwise general linear model (GLM) to determine which environmental factors (oxygen saturation (O_2), temperature (T), and salinity (S) as daily average values per each analyzed period) potentially exerted influence over the univariate diversity indices listed above. GLM is a class of regression models that supports non-normal distributions (Nelder and Wedderburn, 1972) and can be implemented through the R glm() function. Thus, we treated Shannon diversity (H′), Simpson diversity, Pielou's evenness (J′), and species richness (S) for the megabenthic community, and total-traces density (%), surface-trace density (%), relief-trace density (%), total-trace diversity, surface-trace diversity, relief-trace diversity, or trace richness (T) as dependent variables. We used the "vif" function from the "car" package (Fox and Weisberg, 2011) to check for multicollinearity between the explanatory variables, and verified homogeneity and normality of residuals with Shapiro -Wilk and Levene tests, respectively. When data did not meet the assumptions, we performed either $\log_{10}$ or sqrt data transformations. If assumptions were still not met we ran a non-parametric Friedman test.

To investigate variation in multivariate taxonomic community composition among oxygen levels (two levels: hypoxia 1, hypoxia 2) we ran a multivariate analysis of variance (PERMANOVA) performed with 999 random permutations of appropriate units (McArdle and Anderson, 2001). We calculated the resemblance matrices from Bray-Curtis distances of transformed benthic community data, verifying homogeneity of multivariate dispersion using the PERMDISP routine (Anderson et al., 2008).

2.4.2. Sonar data analysis

For the sonar analysis, we also ran stepwise GLM for each of the following dependent variables: number of pits, total bioturbated area, circularity, and diameter of pits. We used oxygen concentration (O_2), temperature, and salinity as environmental predictor variables. Using the same techniques described above, we verified homogeneity and normality of residuals, and once again transformed data in cases that did not meet assumptions. If transformed data still did not meet assumptions, we performed a non-parametric Friedman test, and a post-hoc pairwise Wilcoxon test. When we observed significant differences in dependent variables among the three study periods, we performed post-hoc pairwise Tukey tests.

In order to evaluate hydrodynamic effects on the sediment surface, we ran a linear regression between the width of platform tracks and the time periods of this study. We verified homogeneity of residuals and normality with a Shapiro–Wilk test and a Levene test, respectively. When the data assumptions were not met, we applied a $\log_{10}$ transformation.

All statistical analyses were performed using the package "vegan" (Oksanen et al., 2013) in R software (R Core Team, 2016).

3. Results

The rarefaction curves of both the numbers of observed taxa and total traces showed that the number of videos analyzed in our study generally captured most taxa and traces present in the study area (Fig. 4). The total trace curve in September only did not plateau, indicating incomplete trace sampling (Fig. 4 B).

3.1. Megafaunal community structure from the video camera

The GLM analysis showed multicollinearity between oxygen, temperature, and salinity in relation to megafaunal density and diversity; we therefore chose oxygen as the explanatory variable for further analysis in order to focus on the main research question for this study. However, we acknowledge the difficulty in disentangling our correlated explanatory variables.

We observed 17 counts spanning eight different taxa in May, and 44 counts spanning nine different taxa in September, with significant differences (*t*-test, $p = 0.0001$) in population density between the two bottom-water oxygen conditions. The highest average value (6.3 count $m^{-2} \pm 4.1$ (SD)) occurred in relatively high oxygen concentrations, in contrast to 2.4 count $m^2 \pm 2.4$ (SD) in May under lower oxygen (Supplementary Fig. 3).

Decapod shrimp (Hippolytidae) were the most abundant taxon in both oxygen conditions, in addition to a gastropod, likely belonging to the family Solariellidae, and the pink sea urchin *Strongylocentrotus fragilis* in September. Interestingly, we did not observe *S. fragilis* in May, nor the two sea star taxa, Asteroidea sp., and *Hymenaster* sp. In contrast, we did not observe Paguroidea, Galatheidae crab, and *Eptatretus* sp. in September. (Figs. 5 and 6). Moreover, we observed no significant difference in diversity indices between May and September, with diversity indices slightly greater in September than May, except for Simpson's indices (Table 3).

PERMANOVA revealed no differences between community assemblages for the two bottom-water oxygen concentrations ($F = 1.03$ $p = 0.27$).

3.2. Reworked sediment trace patterns from the video camera

Regarding trace density and diversity analyses, GLM analysis with oxygen, temperature, and salinity as explanatory variables and sediment trace density and diversity as response variables showed multicollinearity among the three explanatory variables. Once again we used oxygen as the primary explanatory variable for further analyses, recognizing the difficulty in disentangling our correlated explanatory variables.

We observed a similar number of total sediment traces for the two oxygen levels, with 74 in May and 75 in September; we also observed that oxygen explained Pielou's evenness only for the total traces during the two time periods we analyzed, but not other diversity indices (Table 4). Representative images of sediment traces in Barkley Canyon Upper Slope are shown in Fig. 7.

Although relief ($n = 74$) and surface traces ($n = 76$) contributed similarly to total traces in May, we observed more surface traces ($n = 118$) than relief traces ($n = 30$) in September, with organism imprints playing a major role in total traces ($n = 44$), followed by depressions ($n = 3$). Among surface traces, we observed *Eptatretus* sp., Galatheidae sp., and Paguroidea sp. imprints only in May. In contrast, we observed traces from *S. fragilis, Hymenaster* sp. and an unidentified worm only in September. We also observed depressions and burrowing sea stars of

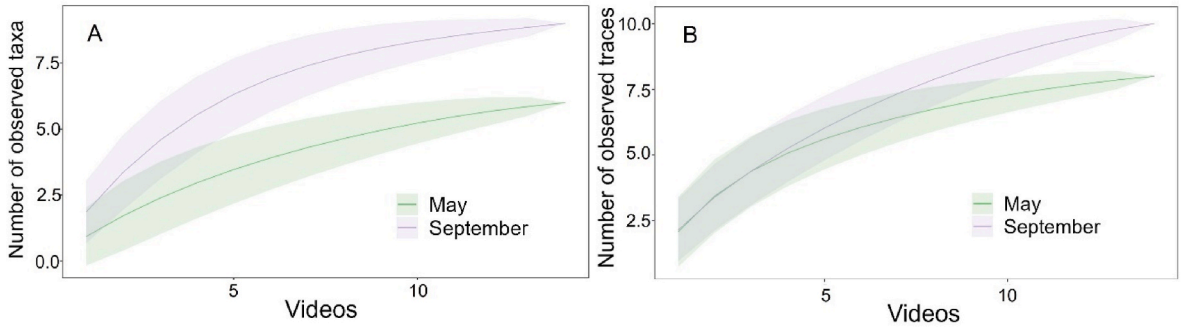

Fig. 4. Rarefaction curves for megafaunal communities (A) and sediment traces (B) in surface sediments per video collected each month (May and September).

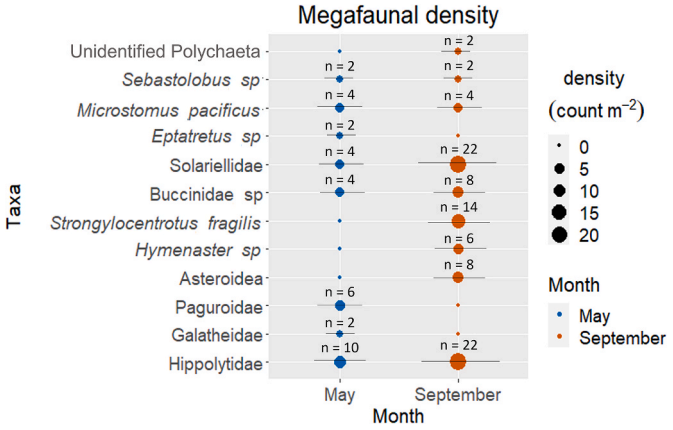

Fig. 5. Averaged density of the observed megafaunal taxonomic groups in May and September, respectively, grouped by species, genera, and families. Error bars represent standard deviation.

both Asteroidea sp. and *Hymenaster* sp. only in September. Regarding relief trace diversity, we observed small and medium burrows at both oxygen levels. However, we observed a higher density of small and medium burrows in May (average 2.3 and 3.1 count m^{-2}) compared to September (1.4 and 0.6 count m^{-2}), when we also observed few large burrows (0.14 count m^{-2}).

The small burrows persisted for a maximum of 1 d under both oxygen conditions. In contrast, the medium burrows persisted for 3–7 d.

In addition, the average total bioturbated area between the two time periods did not differ significantly (lm, F value = 0.06, p = 0.8), varying from ~0.6 m^2 in September to 0.2 m^2 in May. We observed similar values for relief traces of 0.00096 m^2 and 0.00089 m^2, for May and September, respectively. In addition, surface traces in September

Table 3
Average diversity indices (Shannon-Wiener; Simpson; Species richness; Pielou's evenness) during each sampling month, with Friedman test and GLM results for each diversity index.

Month	Shannon-Wiener	Simpson	Species richness	Pielou's evenness
May [O_2] = 0.8 ml l^{-1}	0.35 ± 0.12	0.66 ± 0.10	1.14 ± 0.31	0.49 ± 0.14
September [O_2] = 1.3 ml l^{-1}	0.35 ± 0.13	0.49 ± 0.09	1.86 ± 0.33	0.77 ± 0.10
Friedman test	–	–	–	0.02
GLM (p values)	0.08	0.17	0.12	–

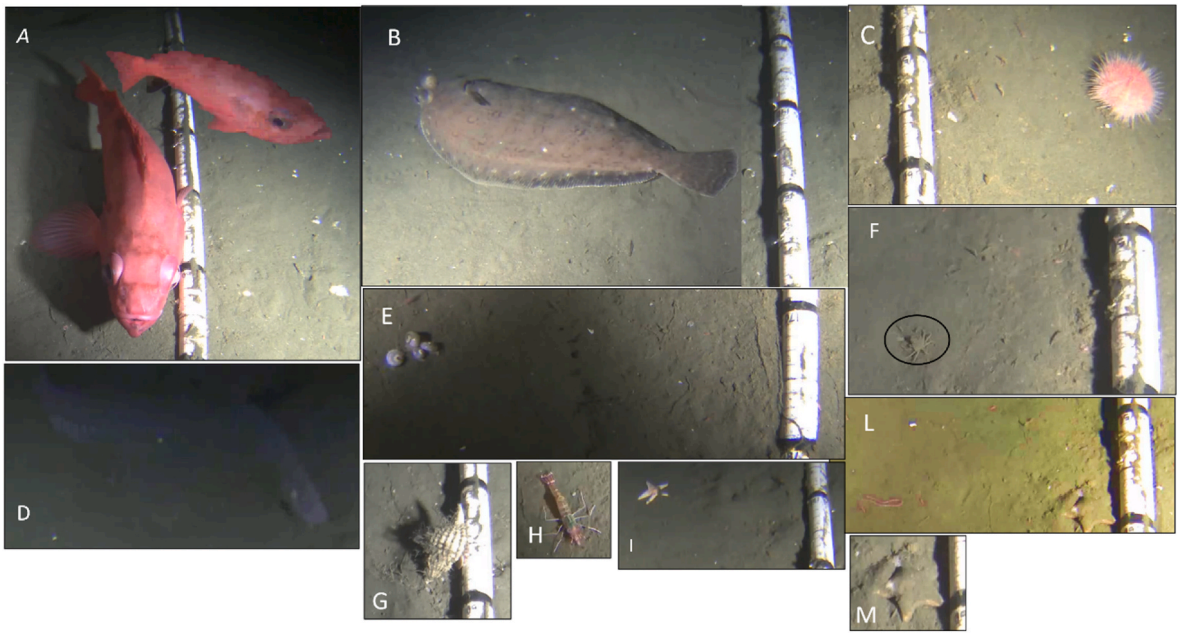

Fig. 6. Photographic examples of the most common taxa in Barkley Canyon Upper Slope observed in May 18–31, and September (20–30), October (1–5) 2023. A) *Sebastes* sp, B) *Microstomus pacificus*, C) *Strongylocentrotus fragilis*., D) *Eptatretus* sp. (the image is dark but the best available), E) Solariellidae sp., F) Galatheidae sp., G) Buccinidae sp., H) Hippolytidae sp., I) Asteroidea sp., L) unidentified Polychaeta, M) *Hymenaster* sp.

Table 4
Results of GLM and Friedman tests showing F-values and p values for each analyzed variable. The first column shows variables included in the analysis (*Variable (J' = Pielou's evenness))*, followed by type of test run (*Test*), F-value (*F-value*) and p-value (*P-value*).

Variable	*Test*	*F-value*	*P-value*
Total trace density	GLM	0.03	0.95
Surface trace density	GLM	3.13	0.08
Relief trace density (log_{10})	GLM	1.10	0.31
Total trace diversity	GLM	0.30	0.60
Surface trace diversity	*GLM*	1.85	0.18
Relief trace diversity[a]	–		–
J' total traces	**Friedman**		**0.02**

[a] Limited number of observations precluded statistical analysis.

covered an area of 1.19 m^2, versus 0.42 m^2 in May.

3.3. Sediment trace patterns from rotary sonar

Our two GLMs showed that the total reworked sediment area differed significantly between the two periods of contrasting bottom-water oxygen concentrations ($p = 0.01$), as did the number of pits ($p < 0.001$), with the highest reworked sediment area and highest number of pits occurring in September (Fig. 8). On average, we counted 298.6 pits and a reworked sediment area of 138.8 m^2 in September, in contrast to 199.9 pits and 99.4 m^2 of the reworked sediment area in low oxygen conditions during May (Fig. 8). In addition, pit diameter averaged 55 cm during both time periods.

We also observed changes in pit shapes concurrently between the two periods of contrasting bottom-water oxygen concentrations when focusing on the entire sonar FOV (Table 5). On average, the circularity descriptor was directly proportional to oxygen levels, specifically, 0.21 in May, 0.24 in September, and 0.25 in December (Fig. 9). However, the size of the pits did not always change significantly when we focused on a specific subsection of the FOV (Fig. 9; Table 5), such as in section 2. In sections 1, 3, and 4, circularity increased from ~0.24 to ~0.35, from May to December (Fig. 9). Diameter did not differ significantly (Friedman test, $p = 0.35$) between different oxygen concentrations (Table 5).

Moreover, examination of sections 1 and 4 showed that the small circularity category (from 0.26 to 0.37) of pits dominated the different oxygen levels/months (see Fig. 10 A, B, C).

In addition, the width size of sediment tracks on the sediment measured in May and September decreased significantly over time (Supplementary Table 2).

4. Discussion

By combining two different imaging techniques, video with a small-scale FOV (~0.5 m^2) versus sonar with a much larger scale FOV (~1268 m^2), we were able to draw a complementary and more detailed interpretation of how different environmental conditions, between May and September 2013, affected sediment reworking processes. Different environmental conditions may reflect different oxygen concentrations near the seafloor which were difficult to disentangle from other biotic and abiotic variables. Whereas we evaluated the role of individual benthic taxa in producing reworked sediment features through bioturbation structures by video imagery, we indirectly assessed the overall levels of biological activity through sonar imagery at BCUS.

The sonar images proved to be the only efficient method for quantifying large reworked sediment traces (pits) and for observing significantly larger areas affected by them during the period of higher bottom-

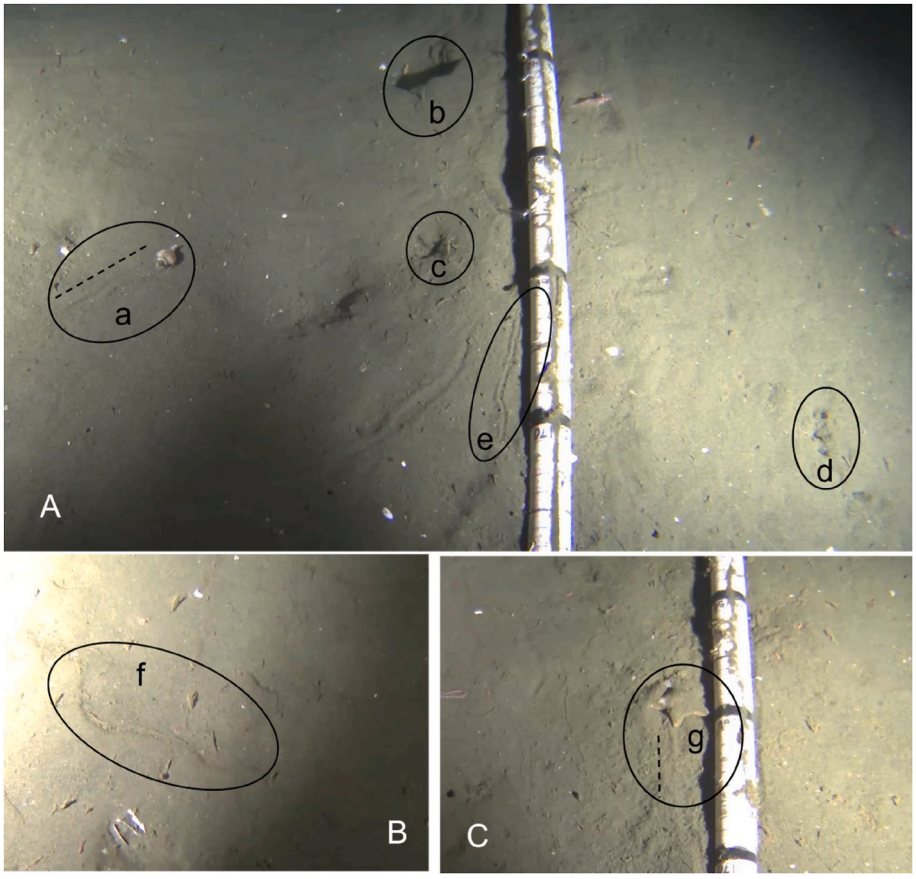

Fig. 7. Representative photographs of bioturbated surface and relief traces in Barkley Canyon Upper Slope from May and September 2013. A) a) Paguroidea trail, b) large burrow, c) medium burrow, d) small burrow, e) single plough. B) f) single plough. C) g) *Hymenaster* sp. trail.

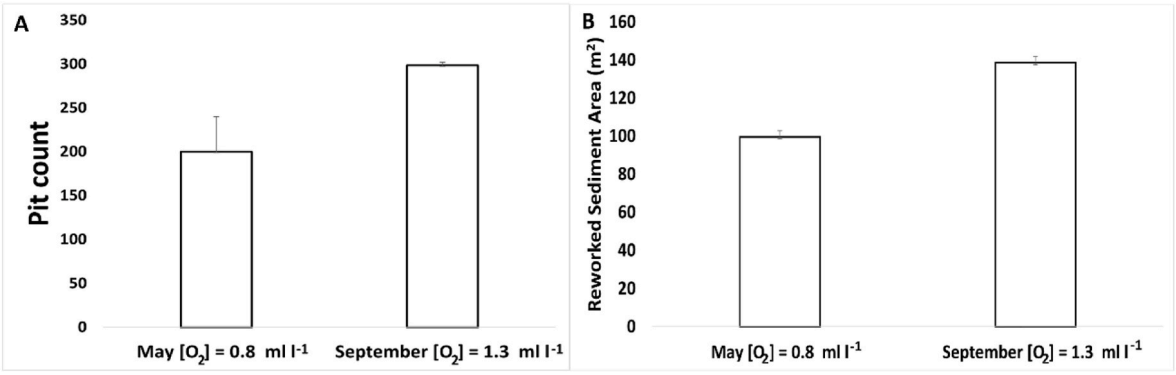

Fig. 8. A) Average number of pits (n = 11 per May and n = 11 per September) and B) reworked sediment area in May and September (based on 11 images per month). Error bars indicate standard deviation.

Table 5
Generalized linear model (GLM), Friedman test (F), and Post-hoc tests (pairwise Wilcoxon test (P–W); Tukey HSD test (THSD)) performed on two pit size descriptors related to the entire FOV, and the fourth selected FOV subsections. *Log_{10} = logarithmic transformation data. Bolded terms indicate significant differences.

		GLM/ Friedman test		Post-hoc test		
	Size descriptors	*Df*	P-value			
Entire FOV (1268.3 m^2)	Circularity	2	**6.6e-15** *(F)*	*(P–W)* May September	December **5.5e-12** 0.6	May – **4.2e-12**
	Diameter	2	0.35 *(F)*	NA		
1st section (~35 m^2)	Circularity	2	**1.4e-08** *(F)*	*(P–W)* May September	December **5.5e-08** 0.6	May – **9.6e-06**
	Diameter	2	0.13 *(F)*	NA		
2nd section (~35 m^2?)	Circularity	2	0.62 *(F)*	NA		
	Diameter	2	0.28 *(F)*	NA		
3rd section (~35 m^2)	Circularity (log_{10})*	2	**6.5e-08** *(glm)*	*(THSD)* May September	December **0.02** **0.002**	May – 0.9
	Diameter	2	0.53 *(F)*	NA		
4th section (~35 m^2	Circularity	2	**1.4e-07** *(F)*	*(P–W)* May September	December **1.9e-06** 0.7	May – **3.5e-06**
	Diameter	2	0.38 *(F)*	NA		

water O_2 concentrations. The pits ranged 40–70 cm in diameter, with smaller pits increasing in number and size over time, indicating increased faunal activity and likely sediment mixing. In parallel, video analysis enabled the identification of similarities and dissimilarities in species composition, including dominant species, but we detected no clear differences in reworked sediment between the two periods of contrasting bottom-water oxygen concentrations. We could also evaluate the average persistence time for each trace, and estimate small-scale reworked sediment area.

4.1. Benthic megafaunal composition

Acknowledging the major role of dissolved oxygen concentration in shaping megafaunal community structure, most marine benthic communities also depend heavily on organic matter supplied from the water column above (Smith et al., 2008). Campanyà-Llovet et al. (2018) showed a stronger influence of OM quantity and quality distribution on macroinfaunal community structure in Barkley Canyon at smaller spatial scales (10s of meters) in contrast to major stressors (i.e., oxygen) that act over larger scales (100s of meters). Campanyà-Llovet et al. (2018) also reported that short-term variability in water mass circulation, such as upwelling and downwelling flows and storm re-suspension events, consistently explained the higher variability within OM composition in Barkley Canyon, with potential effects on the infaunal community. Moreover, Ruhl and Smith (2004) reported an increased abundance of some holothurian species at Station M, 4000 m deep in the Northeast Pacific continental margin, with reduced OM supply, but a positive relationship with POC flux in other species. However, in our study, although megabenthic assemblages did not differ significantly in composition between May and September, densities of some faunal groups were nonetheless three times higher in September, when dissolved oxygen concentration increased by 62%. Nonetheless, we acknowledge the challenges of disentangling the influence of oxygen concentrations on benthic community structure relative to other environmental variables such as temperature, salinity, and OM. Previous studies have established a direct relationship between low oxygen concentrations (hypoxic conditions) and reduced benthic macro- and megafaunal abundance and diversity in oxygen minimum zones (OMZs) (Levin et al., 1991; Levin et al., 2013; Ingole et al., 2010; De Leo et al., 2017). Moreover, Murty et al. (2009) attributed the absence of megafauna in the OMZ core (~400 m depth, $[O_2] = 0.1$ ml l^{-1}) of the Pakistan margin to a critical oxygen threshold ranging 0.15–0.3 ml l^{-1}. However, oxygen thresholds along with a range of other environmental variables (Hunter et al., 1990; Rex and Etter, 1998) vary among species according to their physiology (Pihl et al., 1991; Vetter et al., 1994; Vaquer-Sunyer and Duarte, 2008; Matabos et al., 2014). Hippolytid shrimps were abundant under low bottom-water O_2 conditions in both Barkley Canyon axis (Chauvet et al., 2018) and in a low- O_2 region of the Gulf of Maine (Hendrickx and Hastings, 2007), supporting the idea that hippolytid shrimp tolerate moderate (0.28–0.6 ml l^{-1}) hypoxia. Dissolved O_2 concentrations in our two sampling periods differed by 0.5 ml l^{-1}, and the fauna observed in the video never experienced severe hypoxia, i.e., $[O_2] < 0.5$ ml l^{-1}, (Levin et al., 2001). This relatively modest dissolved O_2 gradient, aligned with the low number of observations, may explain why we observed little difference between benthic assemblages in May and September. Although statistically non-significant, we observed higher megafaunal diversity under higher bottom-water oxygen concentrations. In addition to some taxa in common between May

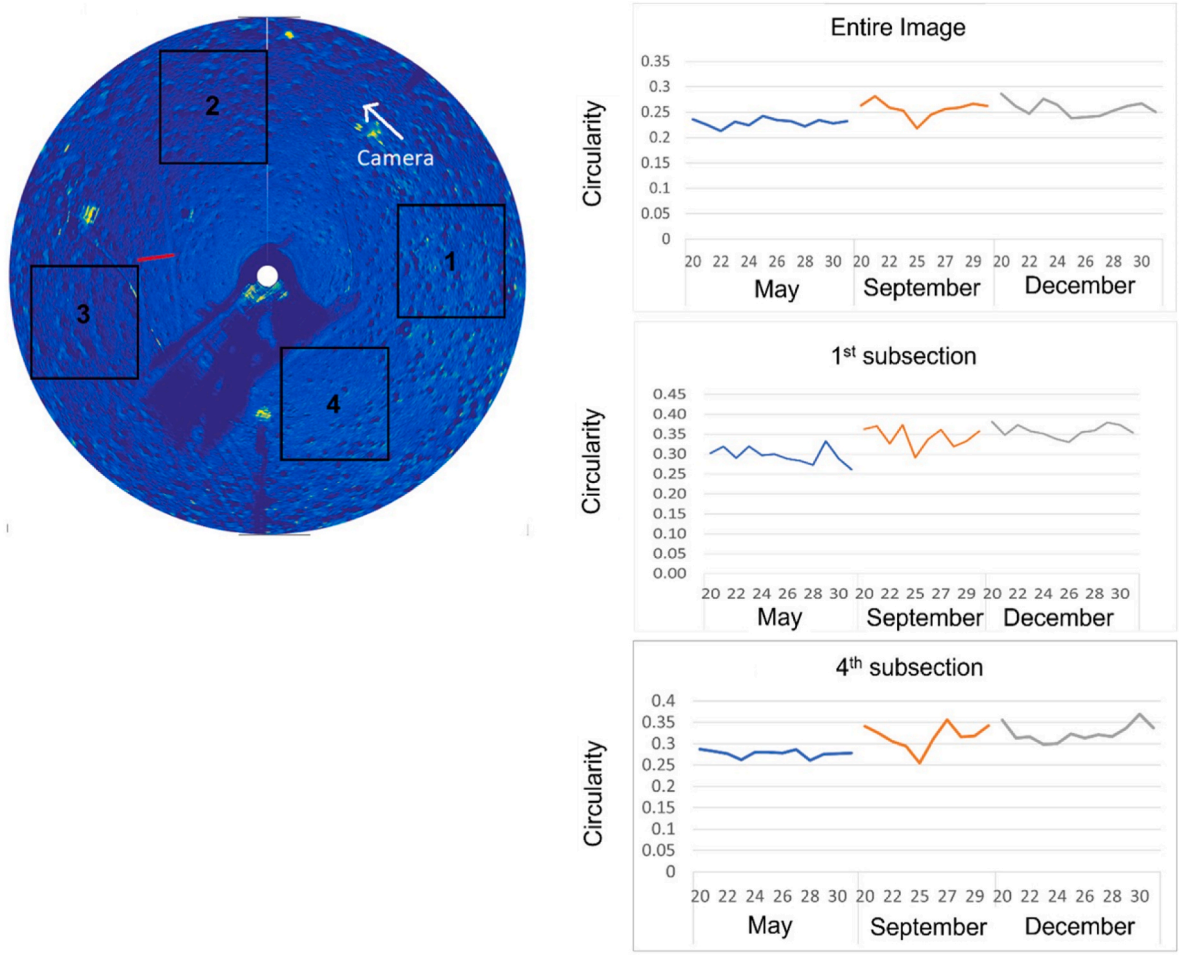

Fig. 9. Left: sonar image overlaid with subsections used in analyses. Right: change in pit circularity (expressed as average circularity) for the entire FOV, and for the first and fourth subsections. The x-axis of each plot indicates the range of time used for our analysis from 20 to 30 d in May, September, and December, respectively. Different color lines in each plot refer to: Blue = May; Orange = September; Gray = December.

and September (e.g., Solariellidae and Buccinidae gastropods, and Hippolytidae shrimps), we also observed unshared taxa such as Paguroidea, Galatheidae crabs, and *Eptatretus* sp. that typified May, whereas *S. fragilis* sea urchins, and the two *Hymenaster* sp., and Asteroidea sea star taxa typified September only. Once again, we were unable to establish a direct relationship between oxygen and megafaunal diversity, but we infer that restricted FOV limited our observations of different species. Murty et al. (2009) observed a bimodal trend in megafaunal diversity along an oxygen and depth gradient and also could not specifically link patterns to oxygen concentrations. Belley et al. (2010) observed no significant difference in macrobenthic species richness between the hypoxic and normoxic stations (>300 m deep) in the St. Lawrence Estuary and the Gulf of St. Lawrence, Canada, respectively. They also reported increased numbers of small surface deposit feeders and an increased abundance of polychaetes tolerant of low oxygen concentrations compared to macrofaunal communities in the 1980s. This pattern was reflected in decreasing species richness, Shannon diversity, and abundance of molluscs, crustaceans, and mobile omnivorous species in the hypoxic region in response to oxygen depletion. In addition, migration could contribute to presence/absence of some species that move to avoid low O_2 concentrations or strong currents that may challenge relatively small-sized organisms such as shrimp (Matabos et al., 2014).

We observed numerous Buccinidae and Solariellidae gastropods, and although the Buccinidae were mostly responsible for surface traces, the Solariellidae, rapid burrower into sediment (Williams et al., 2022), were responsible for the numerous small burrows (based on video observation) that dominated the lowest oxygenated period. Gastropods such as Buccinidae, Solariellidae, and Cymatiidae can tolerate low oxygen concentrations (Theede, 1973) and commonly occur in hypoxic zones, as reported in Barkley Canyon (Chauvet et al., 2018; Command et al., 2023), for species such as *Fusitriton oregonensis* Cymatiidae (De Leo et al., 2017; Domke et al., 2017), and along the Chilean coast (*Jerrybuccinum kantori* Buccinidae, Fraussen et al., 2014).

In contrast to previous work at the same location in years before and after our study (Robert and Juniper, 2012; De Leo et al., 2017; Command et al., 2023) we did not observe strong sea urchin *S. fragilis* and rockfish *Sebastes* spp. dominance, which may also contribute to bioturbation activity through their locomotion in large aggregates that determined sediment resuspension and nutrient cycling (Campanyà-Llovet et al., 2018); *S. fragilis* can remix surface sediments at a rate between 15.1 and 21.0 $m^2\ y^{-1}$ (Robert and Juniper, 2012). We observed only modest numbers (14 count m^{-2}, noting limited number of observations) of *S. fragilis* during the highest bottom-water oxygen period (1.3 ml l^{-1}), but not with lower oxygen concentrations in May. Our results align with De Leo et al. (2017), who reported *S. fragilis* densities up to 2 orders of magnitude higher outside the OMZ (DO ~ 1.4 ml l^{-1}, depth 500–600 m) than inside the OMZ (DO < 0.5 ml l^{-1}) near Vancouver Island. We cannot offer a definitive explanation for the decrease in this species relative to previous studies, but trawling impacts on the British Columbia upper continental slope in 2011 might have altered environmental and particularly biological conditions, changing benthic

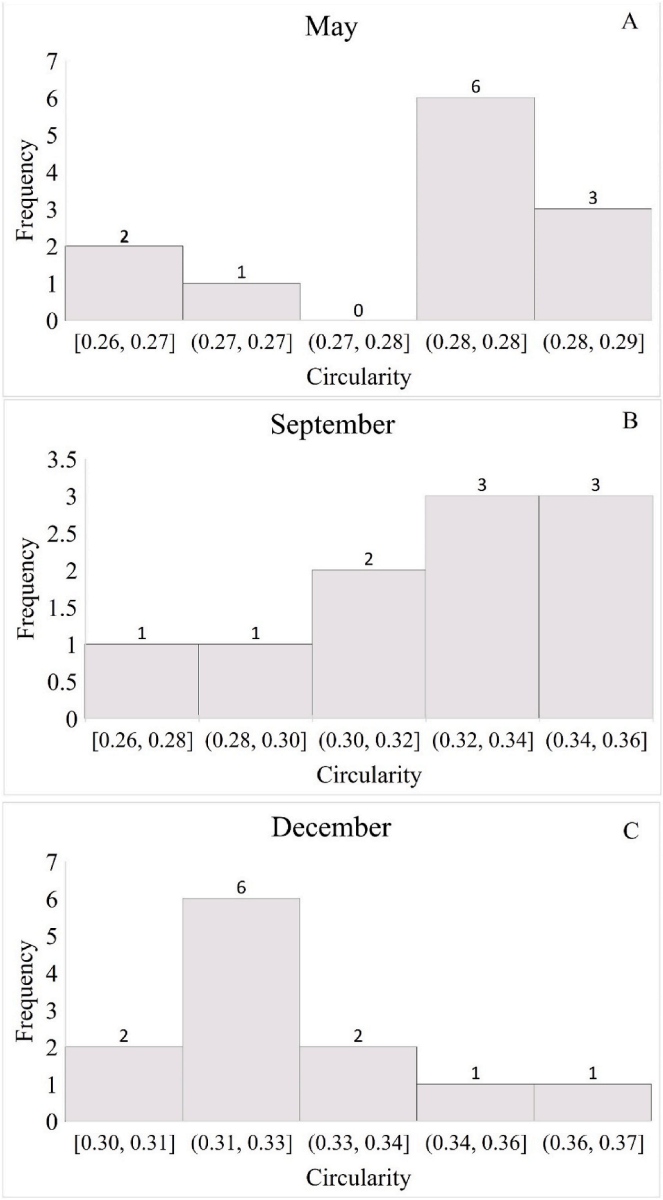

Fig. 10. Histogram showing the distribution of the circularity descriptor (x-axis) among the three different oxygen concentrations/months (A, B, C).

community composition (Puig et al., 2012; De Leo et al., 2017). Although *S. fragilis* can tolerate low oxygen, it nonetheless prefers well-oxygenated environments (Command et al., 2023). The low number of sea urchins in our study could also relate to the longer observation time (1 h; 30 min; and 5 min every second hour) adapted by Robert and Juniper (2012) who used 99 sea urchins to back calculate the area of reworked sediment. Command et al. (2023) also analyzed more video sequences (~480 between September and December 2013) compared to the 246 1-min video sequences we adapted.

Dover sole, *Microstomus pacificus*, a flatfish species known to tolerate hypoxia, depresses its metabolism to limit energy consumption in an environment with low food availability (Vetter et al., 1994). Flatfish, including *M. pacificus*, create depressions as they move around sediments to avoid predators and seek prey (Robert and Juniper, 2012). The ~55 cm diameter pit detected in our sonar images aligns with observations from a previous study (A. Hay, pers. comm.) and might represent a depression created by flatfish; however, unlike Yahel et al. (2008) and Robert and Juniper (2012), we did not observe burrowing flatfish in our visual analysis.

Overall, despite small number of observations and modest differences in oxygen concentrations in our study, our results affirm past studies (e.g., Robert and Juniper, 2012; Chauvet et al., 2018; Command et al., 2023) showing that the environment along Barkley Canyon head (~400 m) and axis (~985 m, characterized by severe hypoxia) hosts benthic organisms such as pink sea urchins, crab *Chionoecetes tanneri*, fish *Anoplopoma fimbria*, mysids (probably *Eucopia* spp.), and buccinid or rannelid gastropods. Those species seem to be physiologically adapted to reduced O_2 concentrations (Levin, 2003; Domke et al., 2017). Therefore, as long as benthic organisms can physiologically adapt to low bottom-water oxygen concentrations and patchy food events, they can maintain populations in Barkley Canyon over time but with low diversity, and with decreasing bioturbation activity. Consequently, benthic ecosystem functioning (e.g., nutrient cycling) linked to bioturbation activity may be modified along with ecosystem services and benefits for humans (Snelgrove et al., 2014).

4.2. *Reworked sediment traces at small scales (video camera)*

Our study showed strong multicollinearity between bottom-water dissolved oxygen, temperature, and salinity as potential drivers of sediment traces in Barkley Canyon sediments. However, bottom-water oxygen saturation did not directly explain sediment trace variability in our video (smaller spatial scale) analysis. Our results mainly support the idea that the OMZ environment (we were unable to disentangle O_2, T, and S definitively) directly affects faunal community structure (i.e., species composition and relative abundances) and indirectly shapes sediment mixing as well as oxygen and nutrient exchange with the sediment given relief traces created by mixing deeper sediment layers and bio-irrigation (Belley et al., 2010). However, the inherent difficulty in reconciling deep sediment mixing solely relying on video observations and relief traces points to a need for further study. Furthermore, the higher density of relief traces with low bottom-water oxygen conditions, as opposed to higher oxygen conditions, contrasts Belley et al. (2010), who reported higher density of surface-traces in the hypoxic region (>300 m deep) of the Lower St. Lawrence Estuary. They attributed this pattern to increased activity by the surface deposit feeder *Ophiura* sp., perhaps reflecting stress behavior in response to hypoxia. In our study, small burrows made by solariellid gastropods dominated relief traces.

Unfortunately, our inability to identify typical Solariellidae burrowing behavior limits our capacity to infer its bioturbation potential. Nevertheless, based on shallow-water studies (Morton, 1990; Cheung et al., 2008), we infer that these gastropods spend most of their time burrowed beneath the sediment surface, emerging only when they detect food at the surface. Thus, although we were unable to measure the depth of small burrows, we infer they move within and mix the upper few centimeters of sediment (Dashtgard and Gingras, 2012), with potential effects on dissolved oxygen penetration into sediments and a continuous sediment mixing at our Barkley Upper Slope site. Moreover, previous studies have suggested gastropods are especially capable and adapted to reworking and breaking apart the less cohesive coarse-grained sediments that compared to mud offer less resistance to burrowing organisms (Dorgan, 2006), which also characterizes Barkley Upper Slope (Campanyà-Lovet et al., 2018). Different sediment bulk densities also may affect animal-sediment interactions. Overall, low bulk density conditions favor macrofaunal movement and sediment reworking (Wiesebron et al., 2021). The overlying sediment exerts an important but non-uniform force on an animal, whether stationary or mobile, facilitating burrowing, as with the solariellid gastropods in our study; Kanazawa (1992) showed that the dome shape of sea urchins living in sand can sustain the downward weight of the sand above them. Therefore, ease of burrowing by gastropods might also explain the rapid turnover (1–3 d) in small burrows compared to large burrows (~7 d) in our study.

We observed a similar proportion of reworked sediment areas

between the two time periods of contrasting bottom-water oxygen, a finding that contrasts previous reports of reduced bioturbation with decreasing oxygen concentration (Diaz and Rosenberg, 1995, 2008; Levin et al., 2009; Middelburg and Levin, 2009). Several factors might explain the similar proportions in our study, including the low number of observations. Alternatively, the larger number of small and medium burrows in May might cover a sediment area similar to the larger surface imprints observed in September. Moreover, we also infer that our video image methodology to evaluate average total reworked sediment area may have influenced our results. The video camera imaged the same FOV as different organisms reworked the same patch of sediment, likely reworking it more than once over the observation period. For example, we observed that a sea star and *S. fragilis* moved through the same patch of sediment repeatedly, however, our analysis counted that area as re-worked only once. Consequently, we potentially over- or under-estimated the bioturbated seafloor area in both study periods. Moreover, larger organisms appeared to be responsible for most surface traces in our study and contributed substantively to local community assemblages, as reported in previous studies (Robert and Juniper, 2012; Belley and Snelgrove, 2017). Robert and Juniper (2012) indicated sediment reworking rates between 26.0 and 35.1 $cm^2\ y^{-1}$ by Dover sole, *M. pacificus*, Pacific halibut, *H. stenolepis,* and the fragile pink sea urchin *S. fragilis.*

In short, our small-spatial scale video analysis enabled coarser investigations of biological aspects of Barkley Canyon Upper Slope under low bottom-water oxygen conditions compared to previous studies that used a larger number of videos. Nonetheless, our analysis provided sufficient information regarding presence/absence of organisms to enable comparisons with concurrent sonar images. Despite the small area of sediment imaged by the video camera, we also demonstrated important contributions of small burrows to sediment mixing in low bottom-water oxygen conditions. Our results indirectly point to the importance of particle reworking in permeable sand, which acts as a biofilter by enhancing particulate organic matter filtration into the sediment and accelerating OM remineralization and nutrient recycling (see also D'Andrea et al., 2004).

4.3. Reworked sediment traces at large scales (sonar)

Previous studies attribute biological pit formation to flatfish as they avoid predators or seek prey (Auster et al., 1995). Although sonar images did not enable species identifications, we infer that the observed increase in the number of pits with increasing bottom-water oxygen concentrations (and the collinear environmental variables) might reflect increasing megafaunal density and differences in assemblage composition during the contrasting sampling periods, as suggested by video analysis. Indeed, although we rarely observed Dover sole, *M. pacificus*, Pacific halibut *H. stenolepis,* and rays such *as Raja rina*, and *Bathyraja* spp., Robert and Juniper (2012) observed them frequently, specifically noting halibut burrowing. Moreover, previous studies documented these two rays leaving oval imprints 6–10 cm deep in the sediment (Howard et al., 1977; Gregory et al., 1979; Thrush et al., 1991; Martinell et al., 2001). Sonar imaging provided valuable information about the extent of seafloor bioturbated area, which increased in September when average bottom-water oxygen concentrations and temperature values increased. However, we again note a need for caution in attributing increasingly reworked sediment to a single environmental factor in our study given the challenges in disentangling O_2, temperature, and salinity and the strong influence that OM might have on bioturbators and organisms.

The species that create burrows also perform a function that benefits other species in that other bioturbators can utilize the burrows, including species that lack the behavioral plasticity or morphological attributes to make their own (Auster et al., 1995; Smith et al., 2000; Levin, 2003; Robert and Juniper, 2012; Thurber et al., 2014). Therefore, burrows play an important ecological function and enhance particle deposition in addition to oxygenating sediments (Yager et al., 1993). Moreover, currents of ~25 cm s^{-1} can affect burrow shape and/or size and consequently promote sediment reworking and organic matter remineralization. Kenyon et al. (2002) showed that bottom currents of 25 cm s^{-1} can move fine-grained sand on the seafloor, the grain size reported by Campanyà-Llovet et al. (2018) for our study area. Indeed, we observed significant increasing circularity over time and across the entire FOV, noting a current of 0–25 cm s^{-1} measured from the Aquadopp profiler. The infilling track information provides evidence of hydrodynamic and bioturbation events that refill the tracks because those activities could also refill pits and influence circularity and shape changes. Moreover, although the data available for this study does not elucidate which factor(s) contributed most to refilling both tracks and pits, we infer that a hydrodynamic event contributed. We observed changes in track width along the entire track rather than specifically at a site as might occur with bioturbation activity. Noting a dearth of previous studies on pit size and shape, we infer that reduced reworking occurs in low bottom-water oxygen conditions that limit most taxa.

In summary, our sonar imagery analysis documented sediment reworking processes over a relatively large scale that varied temporally and spatially, and under different oxygen concentrations that significantly altered bioturbated seabed features. In contrast, video analyses showed no significant effect of different oxygen concentrations on reworked seabed features, likely indicating that different scales of observations influence the evaluation of bioturbation activity. Moreover, our sonar analysis documented the importance of hydrodynamic and biological activity in remixing sediment. The limited FOV of the camera precluded this sort of analysis.

5. Conclusions

Our study provides the first analysis of deep-sea benthic bioturbation activity in the NE Pacific that combines video and sonar images. Using sonar images in particular, we showed that environmental conditions, such as different oxygen concentrations near the seabed, affect sediment reworking. Except for relief burrows, higher reworked sediment generally coincided with higher bottom-water oxygen concentrations, though not significantly; this trend corroborates past OMZ studies that link faunal abundance, diversity, and activity to an oxygen gradient. Moreover, our study illustrates the complementarity of video and sonar imaging systems, noting that the absence of one would not have allowed us to study the full range of sediment features that the second instrument could not document. Despite the limited number of observations, video imagery allowed us to investigate megafaunal distributions and the role of small burrows in sediment remixing, whereas sonar documented bioturbation pit distribution and increases in pit size as oxygen levels increased. We also note the critical importance of selection of appropriate spatial scales when defining a sampling methodology to investigate bioturbation activity. We then recognize the need for improvements when combining video and sonar imaging. For example, future studies could mount a sonar and camera near the seafloor in such a way that their FOVs partially overlap, therefore simultaneously sampling and comparing benthic habitat and fauna directly. Thus, we can observe a species through video images, study its location through spatial coordinates, infer its presence from reflected sonar images, and identify the biological bedform that the species left. However, different species can create pits with similar shapes and different species can reuse a given pit. This ambiguity points to a need for further studies. We conclude by suggesting that the combined use of both video and sonar images will enable future studies that enhance knowledge of benthic ecosystems at larger scales than possible with fixed-point video imagery alone.

CRediT authorship contribution statement

Alessia C. Ciraolo: Conceptualization, Data curation, Methodology, Writing – original draft, Writing – review & editing. **Paul V.R.**

Snelgrove: Conceptualization, Supervision, Writing – review & editing. **Douglas Schillinger:** Conceptualization, Methodology, Writing – review & editing. **Fabio C. De Leo:** Conceptualization, Writing – review & editing.

Declaration of competing interest

The authors declare that they have no known competing financial interests or personal relationships that could have appeared to influence the work reported in this paper.

Data availability

Data will be made available on request.

Acknowledgments

Ocean Networks Canada is funded through the Canada Foundation for Innovation-Major Science Initiative (CFI-MSI) fund 30199. We are thankful for the support from ONC's marine and digital operations staff for servicing and maintaining the NEPTUNE observatory and for the curation and quality control of all oceanographic data streams used in this study. We thank Dr. Jacopo Aguzzi for providing suggestions on the oblique perspective grid, and Azeez Sarafadeen, for help with the video analysis. Drs. Amanda Bates, Suzanne Dufour, Jasmin Godbold, Duncan McIlroy Evan Edinger, and three anonymous reviewers provided very helpful comments on on earlier versions of this manuscript. This research was sponsored by the Natural Sciences and Engineering Research Council of Canada (NSERC). We also thank the School of Graduate Studies at Memorial University for additional financial support.

Appendix A. Supplementary data

Supplementary data to this article can be found online at https://doi.org/10.1016/j.dsr.2024.104236.

References

Aguzzi, J., Chatzievangelou, D., Marini, S., Fanelli, E., Danovaro, R., et al., 2019. New high-tech flexible networks for the monitoring of deep-sea ecosystems. Environ. Sci. Technol. 53 (12), 6616–6631.

Aguzzi, J., Chatzievangelou, D., Francescangeli, M., Marini, S., Bonofiglio, F., et al., 2020. The hierarchic treatment of marine ecological information from spatial networks of benthic platforms. Sensors 20 (6), 1751.

Anderson, M., Gorley, R., Clarke, K.P., 2008. For PRIMER : Guide to Software and Statistical Methods. Primer-e, Plymouth, UK, p. 32.

Auster, P.J., Malatesta, R.J., LaRosa, S.C., 1995. Patterns of microhabitat utilization by mobile megafauna on the southern New England (USA) continental shelf and slope. Mar. Ecol. Prog. Ser. 127, 77–85.

Barnes, C.R., Best, M.M.R., Bornhold, B.D., Juniper, S.K., Pirenne, B., et al., 2007. The NEPTUNE Project-a cabled ocean observatory in the NE Pacific: overview, challenges and scientific objectives for the installation and operation of Stage I in Canadian waters. In: Symposium on Underwater Technology and Workshop on Scientific Use of Submarine Cables and Related Technologies, pp. 308–313.

Bell, J.B., Jones, D.O., Alt, C.H., 2013. Lebensspuren of the bathyal mid-Atlantic ridge. Deep Sea Res. Part II 98, 341–351.

Belley, R., Snelgrove, P.V.R., 2017. The role of infaunal functional and species diversity in short-term response of contrasting benthic communities to an experimental food pulse. J. Exp. Mar. Biol. Ecol. 491, 38–50.

Belley, R., Archambault, P., Sundby, B., Gilbert, F., Gagnon, J.M., 2010. Effects of hypoxia on benthic macrofauna and bioturbation in the Estuary and Gulf of St. Lawrence, Canada. Continent. Shelf Res. 30 (12), 1302–1313.

Cadée, G.C., 1976. Sediment reworking by *Arenicola marina* on tidal flats in the Dutch Wadden Sea. Neth. J. Sea Res. (4).

Campanyà-Llovet, N., Snelgrove, P.V.R., Parrish, C.C., 2017. Rethinking the importance of food quality in marine benthic food webs. Prog. Oceanogr. 156, 240–251.

Campanyà-Llovet, N., Snelgrove, P.V.R., De Leo, F.C., 2018. Food quantity and quality in Barkley Canyon (NE Pacific) and its influence on macroinfaunal community structure. Prog. Oceanogr. 169, 106–119.

Chauvet, P., Metaxas, A., Hay, A.E., Matabos, M., 2018. Annual and seasonal dynamics of deep-sea megafaunal epibenthic communities in Barkley Canyon (British Columbia, Canada): a response to climatology, surface productivity and benthic boundary layer variation. Prog. Oceanogr. 169, 89–105.

Cheung, S.G., Chan, H.Y., Liu, C.C., Shin, P.K.S., 2008. Effect of prolonged hypoxia on food consumption, respiration, growth and reproduction in marine scavenging gastropod *Nassarius festivus*. Mar. Pollut. Bull. 57 (6–12), 280–286.

Command, R., De Leo, F.C., Robert, K., 2023. Temporal dynamics of the deep-sea pink urchin *Strongylocentrotus fragilis* on the Northeast Pacific continental margin. Deep-Sea Res. I 193. https://doi.org/10.1016/j.dsr.2022.103958.

Dashtgard, S.E., Gingras, M.K., 2012. Marine invertebrate neoichnology. Sedimentology 64, 273–295. Elsevier.

De Leo, F.C., Gauthier, M., Nephin, J., Mihaly, S., Juniper, S.K., 2017. Bottom trawling and oxygen minimum zone influences on continental slope benthic community structure off Vancouver Island (NE Pacific). Deep Sea Res. Part II Top. Stud. Oceanogr. 137, 404–419.

De Leo, F.C., Ogata, B., Sastri, A.R., Heesemann, M., Mihály, S., et al., 2018. High-frequency observations from a deep-sea cabled observatory reveal seasonal overwintering of *Neocalanus* spp. in Barkley Canyon, NE Pacific: insights into particulate organic carbon flux. Prog. Oceanogr. 169, 120–137.

Diaz, R.J., Rosenberg, R., 1995. Marine benthic hypoxia: a review of its ecological effects and the behavioural responses of benthic macrofauna. Oceanogr. Mar. Biol. Annu. Rev. 33, 245-03.

Diaz, R.J., Rosenberg, R., 2008. Spreading dead zones and consequences for marine ecosystems. Science 321 (5891), 926–929.

Domke, L., Lacharité, M., Metaxas, A., Matabos, M., 2017. Influence of an oxygen minimum zone and macroalgal enrichment on benthic megafaunal community composition in a NE Pacific submarine canyon. Mar. Ecol. Prog. Ser. 38 (6), e12481.

Dorgan, K.M., 2006. Macrofaunal burrowing: the medium is the message. Oceanogr. Mar. Biol. Annu. Rev. 48, 85–121.

DuVal, C.B., Trembanis, A.C., Miller, D.C., 2021. A regime-state framework for morphodynamic modeling of seabed roughness. J. Geophys. Res. Oceans 126 (5), e2020JC016769.

D'Andrea, A.F., Lopez, G.R., Aller, R.C., 2004. Rapid physical and biological particle mixing on an intertidal sandflat. J. Mar. Res. 62 (1), 67–92.

Ekau, W., Auel, H., Pörtner, H.O., Gilbert, D., 2010. Impacts of hypoxia on the structure and processes in pelagic communities (zooplankton, macro-invertebrates and fish). Biogeosciences 7 (5), 1669–1699.

Fox, J., Weisberg, S., 2011. An {R} Companion to Applied Regression, 2 Edition.

Fraussen, K., Sellanes, J., Stahlschmidt, P., 2014. The South American radiation of *Jerrybuccinum* (Gastropoda, Buccinidae), with a new deep-water species from Chile. ZooKeys (409), 61.

Furukawa, Y., Bentley, S.J., Lavoie, D.L., 2001. Bioirrigation modeling in experimental benthic mesocosms. J. Mar. Res. 59 (3), 417–452.

Gregory, M.R., Ballance, P.F., Gibson, G.W., Ayling, A.M., 1979. On how some rays (Elasmobranchia) excavate feeding depressions by jetting water. J. Sediment. Res. 49 (4), 1125–1129.

Hay, A.E., Wilson, D.J., 1994. Rotary sidescan images of nearshore bedform evolution during a storm. Mar. Geol. 119 (1–2), 57–65.

Hendrickx, M.E., Hastings, P.A., 2007. Ecological data for *Myxine circifrons* garman, 1899 (myxiniformes: myxinidae) in the Gulf of California, Mexico. HIDROBIOLOGICA 17 (3), 273–276.

Howard, J., Mayou, T., Heard, R., 1977. Biogenic sedimentary structures formed by rays. Jour. Sed. 47 (1), 339–346.

Huettel, M., Webster, I.T., 2001. Porewater flow in permeable sediments. In: Boudreau, B.P., et al. (Eds.), The Benthic Boundary Layer: Transport Processes and Biogeochemistry, pp. 144–177.

Hunter, J.R., Butler, J.L., Kimbrell, C., Lynn, E.A., 1990. Bathymetric patterns in size, age, sexual maturity, water content, and caloric density of Dover sole, *Microstomus pacificus*. CalCOFI Invest. Rep 31, 132–144.

Ingole, B.S., Sautya, S., Sivadas, S., Singh, R., Nanajkar, M., 2010. Macrofaunal community structure in the western Indian continental margin including the oxygen minimum zone. Mar. Ecol. Prog. Ser. 31 (1), 148–166.

Jones, K.R., Traykovski, P., 2018. A method to quantify bedform height and asymmetry from a low-mounted sidescan sonar. J. Atmos. Ocean. Technol. 35 (4), 893–910.

Jones, D.O., Bett, B.J., Tyler, P.A., 2007. Megabenthic ecology of the deep Faroe–Shetland channel: a photographic study. Deep-Sea Res. Part I Oceanogr. Res. Pap. 54 (7), 1111–1128.

Kanazawa, K.I., 1992. Adaptation of test shape for burrowing and locomotion in spatangoid echinoids. Paleontology 35 (4), 733–750.

Kenyon, N.H., Akhmetzhanov, A.M., Twichell, D.C., 2002. Sand wave fields beneath the Loop Current, Gulf of Mexico: reworking of fan sands. Mar. Geol. 192 (1–3), 297–307.

Kristensen, E., 2000. Organic matter diagenesis at the oxic/anoxic interface in coastal marine sediments, with emphasis on the role of burrowing animals. Life at interfaces and under extreme conditions. Hydrobiologia 426 (1), 1–24.

Kristensen, E., Penha-Lopes, G., Delefosse, M., Valdemarsen, T., Quintana, C.O., et al., 2012. What is bioturbation? The need for a precise definition for fauna in aquatic sciences. Mar. Ecol. Prog. Ser. 446, 285–302.

Kukert, H., Smith, C.R., 1992. Disturbance, colonization and succession in a deep-sea sediment community: artificial-mound experiments. Deep-Sea Res. Part I Oceanogr. Res. Pap. 39 (7–8), 1349–1371.

Lamarque, B., Deflandre, B., Galindo Dalto, A., Schmidt, S., Romero-Ramirez, A., et al., 2021. Spatial distributions of surface sedimentary organics and sediment profile image characteristics in a high-energy temperate marine RiOMar: the West gironde mud patch. J. Mar. Sci. Eng. 9 (3), 242.

Levin, L.A., 2003. Oxygen minimum zone benthos: adaptation and community response to hypoxia. Oceanogr. Mar. Biol. Annu. Rev. 41, 1–45.

Levin, L.A., Huggett, C.L., Wishner, K.F., 1991. Control of deep-sea benthic community structure by oxygen and organic-matter gradients in the eastern Pacific Ocean. J. Mar. Res. 49 (4), 763–800.
Levin, L.A., Etter, R.J., Rex, M.A., Gooday, A.J., Smith, C.R., et al., 2001. Environmental influences on regional deep-sea species diversity. Annu. Rev. Ecol. Systemat. 32, 51–93.
Levin, L.A., Ekau, W., Gooday, A.J., Jorissen, F., Middelburg, J.J., 2009. Effects of natural and human-induced hypoxia on coastal benthos. Biogeosciences 6 (10), 2063–2098.
Levin, L.A., McGregor, A.L., Mendoza, G.F., Woulds, C., Cross, P., et al., 2013. Macrofaunal colonization across the Indian Margin oxygen minimum zone. Biogeosciences 10 (11), 7161–7177.
Lopez-Vazquez, V., Lopez-Guede, J.M., Marini, S., Fanelli, E., Johnsen, E., et al., 2020. Video image enhancement and machine learning pipeline for underwater animal detection and classification at cabled observatories. Sensors 20 (3), 726.
Maier, I., Hay, A.E., 2009. Occurrence and orientation of anorbital ripples in near-shore sands. J. Geophys. Res. 114 (F4).
Maire, O., Lecroart, P., Meysman, F., Rosenberg, R., Duchêne, J.C., et al., 2008. Quantification of sediment reworking rates in bioturbation research: a review. Aquat. Biol. 2 (3), 219–238.
Martinell, J., De Gibert, J.M., Domènech, R., Ekdale, A.A., Steen, P.P., 2001. Cretaceous ray Traces? an alternative interpretation for the alleged dinosaur tracks of La Posa, Isona, NE Spain. Palaios 16 (4), 409–416.
Matabos, M., Bui, A.O., Mihály, S., Aguzzi, J., Juniper, S.K., et al., 2014. High-frequency study of epibenthic megafaunal community dynamics in Barkley Canyon: a multi-disciplinary approach using the NEPTUNE Canada network. J. Mar. Syst. 130, 56–68.
Mauviel, A., Sibuet, M., 1985. Répartition des traces animals et importance de la bioturbation. In: Peuplements profonds du Golfe de Gascogne: Campagnes BIOGAS. IFREMER, pp. 157–173.
McArdle, B.H., Anderson, M.J., 2001. Fitting multivariate models to community data: a comment on distance-based redundancy analysis. Ecology 82 (1), 290–297.
Miatta, M., Snelgrove, P.V.R., 2021. Benthic nutrient fluxes in deep-sea sediments within the Laurentian Channel MPA (eastern Canada): the relative roles of macrofauna, environment, and sea pen octocorals. Deep-Sea Res. I: Oceanogr. Res. Pap. 178, 103655.
Middelburg, J.J., Levin, L.A., 2009. Coastal hypoxia and sediment biogeochemistry. Biogeosciences 6 (7), 1273–1293.
Morton, B., 1990. The physiology and feeding behaviour of two marine scavenging gastropods in Hong Kong: the subtidal *Babylonia lutosa* (Lamarck) and the intertidal *Nassarius festivus* (Powys). J. Molluscan Stud. 56 (2), 275–288.
Murty, S.J., Bett, B.J., Gooday, A.J., 2009. Megafaunal responses to strong oxygen gradients on the Pakistan margin of the Arabian Sea. Deep Sea Res. Part II Top. Stud. Oceanogr. 56 (6–7), 472–487.
Nelder, J.A., Wedderburn, R.W., 1972. Generalized linear models. J. R. Stat. Soc. Ser. A Stat. Soc. 135 (3), 370–384.
Nowell, A.R., Jumars, P.A., Fauchald, K., 1984. The foraging strategy of a subtidal and deep-sea deposit feeder 1. Limnol. Oceanogr. 29 (3), 645–649.
Oksanen, J., Blanchet, F.G., Kindt, R., Legendre, P., et al., 2013. Vegan: Community Ecology Package. R Package Version 2.0-10. http://CRAN.Rproject.org/package=vegan.
Pihl, L., Baden, S.P., Diaz, R.J., 1991. Effects of periodic hypoxia on distribution of demersal fish and crustaceans. Mar. Biol. 108, 349–360.
Puig, P., Canals, M., Company, J.B., Martín, J., Amblas, D., et al., 2012. Ploughing the deep-sea floor. Nature 489 (7415), 286–289.
R Core Team, 2016. R: A Language and Environment for Statistical Computing. Vienna, Austria. https://www.R-project.org/.
Rasband, W.S., 1997-2018. ImageJ. U. S. National Institutes of Health, Bethesda, Maryland, USA. https://imagej.nih.gov/ij/.
Rex, M.A., Etter, R.J., 1998. Bathymetric patterns of body size: implications for deep-sea biodiversity. Deep Sea Res. Part II Top. Stud. Oceanogr. 45 (1–3), 103–127.
Rhoads, D.C., 1963. Rates of sediment reworking by *Yoldia limatula* in buzzards bay, Massachusetts, and long Island sound. J. Sediment. Res. 33 (3), 723–727.
Rhoads, D.C., Cande, S., 1971. Sediment profile camera for in situ study of organism-sediment relations 1. Limnol. Oceanogr. 16 (1), 110–114.
Riedel, B., Pados, T., Pretterebner, K., Schiemer, L., Steckbauer, et al., 2014. Effect of hypoxia and anoxia on invertebrate behaviour: ecological perspectives from species to community level. Biogeosciences 11 (6), 1491–1518.
Robert, K., Juniper, S.K., 2012. Surface-sediment bioturbation quantified with cameras on the NEPTUNE Canada cabled observatory. Mar. Ecol. Prog. Ser. 453, 137–149.
Romero-Ramirez, A., Grémare, A., Bernard, G., Pascal, L., Maire, O., et al., 2016. Development and validation of a video analysis software for marine benthic applications. J. Mar. Syst. 162, 4–17.
Ruhl, H.A., Smith, J.K.L., 2004. Shifts in deep-sea community structure linked to climate and food supply. Science 305 (5683), 513–515.
Seike, K., Jenkins, R.G., Watanabe, H., Nomaki, H., Sato, K., 2012. Novel use of burrow casting as a research tool in deep-sea ecology. Biol. Lett. 8 (4), 648–651.
Shull, D.H., 2009. Bioturbation. Ocean Sci. 3, 671–676.
Shum, K.T., Sundby, B., 1996. Organic matter processing in continental shelf sediments—the subtidal pump revisited. Mar. Chem. 53 (1–2), 81–87.
Smith, C.R., Levin, L.A., Hoover, D.J., McMurtry, G., Gage, J.D., 2000. Variations in bioturbation across the oxygen minimum zone in the northwest Arabian Sea. Deep Sea Res. Part II Top. Stud. Oceanogr. 47 (1–2), 227–257.
Smith, C.R., De Leo, F.C., Bernardino, A.F., Sweetman, A.K., Arbizu, P.M., 2008. Abyssal food limitation, ecosystem structure and climate change. Trends Ecol. Evol. 23 (9), 518–528.
Smith, L.M., Cimoli, L., LaScala-Gruenewald, D., Pachiadaki, M., Phillips, B., et al., 2022. The deep ocean observing strategy: addressing global challenges in the deep sea through collaboration. Mar. Technol. Soc. J. 56 (3), 50–66.
Snelgrove, P.V.R., Thrush, S.F., Wall, D.H., Norkko, A., 2014. Real world biodiversity–ecosystem functioning: a seafloor perspective. Trends Ecol. Evol. 29 (7), 398–405.
Solan, M., Kennedy, R., 2002. Observation and quantification of in situ animal-sediment relations using time-lapse sediment profile imagery (t-SPI). Mar. Ecol. Prog. Ser. 228, 179–191.
Solan, M., Wigham, B.D., Hudson, I.R., Kennedy, R., Coulon, C.H., et al., 2004. In situ quantification of bioturbation using time lapse fluorescent sediment profile imaging (f SPI), luminophore tracers and model simulation. Mar. Ecol. Prog. Ser. 271, 1–12.
Sturdivant, S.K., Diaz, R.J., Cutter, G.R., 2012. Bioturbation in a declining oxygen environment, in situ observations from Wormcam. PLoS One 7 (4), e34539.
Sweetman, A.K., Witte, U., 2008. Response of an abyssal macrofaunal community to a phytodetrital pulse. Mar. Ecol. Prog. Ser. 355, 73–84.
The GIMP Development Team, 2019. GIMP. Retrieved from. https://www.gimp.org.
Theede, H., 1973. Comparative studies on the influence of oxygen deficiency and hydrogen sulphide on marine bottom invertebrates. Neth. J. Sea Res. 7, 244–252.
Thomsen, L., Aguzzi, J., Costa, C., De Leo, F., Ogston, A., et al., 2017. The oceanic biological pump: rapid carbon transfer to depth at continental margins during winter. Sci. Rep. 7 (1), 1–10.
Thrush, S.F., Pridmore, R.D., Hewitt, J.E., Cummings, V.J., 1991. Impact of ray feeding disturbances on sandflat macrobenthos: do communities dominated by polychaetes or shellfish respond differently? Mar. Ecol. Prog. Ser. 69 (3), 245–252.
Thurber, A.R., Sweetman, A.K., Narayanaswamy, B.E., Jones, D.O., Ingels, J., et al., 2014. Ecosystem function and services provided by the deep sea. Biogeosciences 11 (14), 3941–3963.
Vaquer-Sunyer, R., Duarte, C.M., 2008. Thresholds of hypoxia for marine biodiversity. Proc. Natl. Acad. Sci. USA 105 (40), 15452–15457.
Vardaro, M.F., Bagley, P.M., Bailey, D.M., Bett, B.J., et al., 2013. A Southeast Atlantic deep-ocean observatory: first experiences and results. Limnol Oceanogr. Methods 11 (6), 304–315.
Vetter, R.D., Lynn, E.A., Garza, M., Costa, A.S., 1994. Depth zonation and metabolic adaptation in Dover sole, *Microstomus pacificus*, and other deep-living flatfishes: factors that affect the sole. Mar. Biol. 120 (1), 145–159.
Wheatcroft, R.A., 1991. Conservative tracer study of horizontal sediment mixing rates in a bathyal basin, California borderland. J. Mar. Res. 49 (3), 565–588.
Wiesebron, L.E., Steiner, N., Morys, C., Ysebaert, T., Bouma, T.J., 2021. Sediment bulk density effects on benthic macrofauna burrowing and bioturbation behavior. Front. Mar. Sci. 8, 707785.
Williams, S.T., Noone, E.S., Smith, L.M., Sumner-Rooney, L., 2022. Evolutionary loss of shell pigmentation, pattern, and eye structure in deep-sea snails in the dysphotic zone. Evolution 76 (12), 3026–3040.
Witte, U., Aberle, N., Sand, M., Wenzhöfer, F., 2003. Rapid response of a deep-sea benthic community to POM enrichment: an in situ experimental study. Mar. Ecol. Prog. Ser. 251, 27–36.
Yager, P.L., Nowell, A.R., Jumars, P.A., 1993. Enhanced deposition to pits: a local food source for benthos. J. Mar. Res. 51 (1), 209–236.
Yahel, G., Yahel, R., Katz, T., Lazar, B., Herut, B., et al., 2008. Fish activity: a major mechanism for sediment resuspension and organic matter remineralization in coastal marine sediments. Mar. Ecol. Prog. Ser. 372, 195–209.